Journal of Power Sources 196 (2011) 3664–3668

Contents lists available at ScienceDirect

Journal of Power Sources

journal homepage: www.elsevier.com/locate/jpowsour

Short communication

Atomistic mechanisms of lithium insertion in amorphous silicon

Shan Huang, Ting Zhu*

Woodruff School of Mechanical Engineering, Georgia Institute of Technology, 801 Ferst Dr. NW, Atlanta, GA 30332, USA

ARTICLE INFO

Article history:
Received 13 October 2010
Received in revised form
28 November 2010
Accepted 29 November 2010
Available online 4 December 2010

Keywords:
Battery
Lithium
Atomistic modeling
Silicon
Electrochemically driven solid state amorphization

ABSTRACT

Understanding the lithium–silicon alloying behavior is essential for achieving maximum charge capacity in the negative electrodes of lithium-ion batteries. Our atomistic simulations show that in amorphous silicon with a disordered network structure, inserted lithium atoms can find equilibrium positions in the interstices of big rings. Alternatively, lithium is incorporated into the network by the destruction and reformation of smaller rings. These atomic-level mechanisms are characterized by using the network topology measure of ring statistics, which are correlated to the lithiation responses of silicon electrodes. The results reveal the influence of lithium concentrations on the electro-chemical–mechanical behavior of silicon. Implications on the reversibility and dynamics of the lithiation process are discussed.

1. Introduction

Rechargeable lithium-ion batteries are currently the preferred form of electrical energy storage devices [1,2]. They can deliver high energy density (~210 Wh kg^{-1}; 650 Wh l^{-1}) with long life cycle. Their recent and potential applications include portable electronic devices, cordless power tools, and electric vehicles. Silicon is being considered as an anode material for Li-ion batteries because it has the highest known theoretical charge capacity (4200 mAh g^{-1}) [3–8]. However, Si anodes often suffer from pulverization and capacity fading. This is caused by the large volume changes of Si (~300%) upon Li insertion/extraction close to its theoretical charge/discharge limit. This issue is particularly significant when the Si electrodes are subject to high-rate charging or discharging, which is highly desirable but often induces a non-uniform distribution of Li in Si. The resulting large incompatible deformation between areas of different Li contents tends to initiate fracture, leading to the electro-chemical–mechanical failure of Si electrodes [9–11]. Are there new ways to optimize the charge capacity of Si anodes while preventing failures? To address this question, understanding the Li–Si alloying behavior is essential, requiring fundamental research that goes beyond empirical battery cell studies.

Metastable amorphous glass is formed when the crystallization of intermediate compounds is frustrated [4]. When reacted with Li, Si crystals yield solid-state amorphous phases at low temperature, but crystalline phases at high temperature (415 °C) [12]. The formation of amorphous Li_xSi alloys, where x denotes the ratio of Li–Si, has been experimentally observed at room-temperature in the electrochemical reactions of Li with Si thin films [4], nanoparticles [5] and nanowires [6]. In principle, amorphous Li_xSi avoids the formation of coherent boundaries between coexisting crystalline phases of different Li concentrations. This can mitigate the buildup of incompatible strains (and thus internal stresses) in Si electrodes so as to improve the cycling performance of batteries. In addition, a variety of Si nanostructure morphologies have been explored to enable Si to perform well as anodes [5–7], as it is supposed that the nanometer size scale can facilitate strain relaxation, enhance flaw tolerance [13], shorten diffusion path, and increase surface area of Si to better react with Li.

As a fundamental step towards understanding the Li–Si alloying behavior, here we report an atomic-level study of Li insertion in amorphous Si (*a*-Si). The structures and energetics of Li–Si alloys are computed quantum-mechanically by using the molecular orbital theory [14]. Detailed analyses of the ring geometry and statistics are related to various electro-chemical–mechanical characteristics of Li reactions with *a*-Si. They are found to depend sensitively on the local Li concentration. The results provide an atomistic basis for further study of the dynamic alloying processes and electrochemically driven solid state amorphization between Li and Si.

* Corresponding author. Tel.: +1 404 894 6597; fax: +1 404 894 0186.
E-mail address: ting.zhu@me.gatech.edu (T. Zhu).

0378-7753/$ – see front matter © 2010 Elsevier B.V. All rights reserved.
doi:10.1016/j.jpowsour.2010.11.155

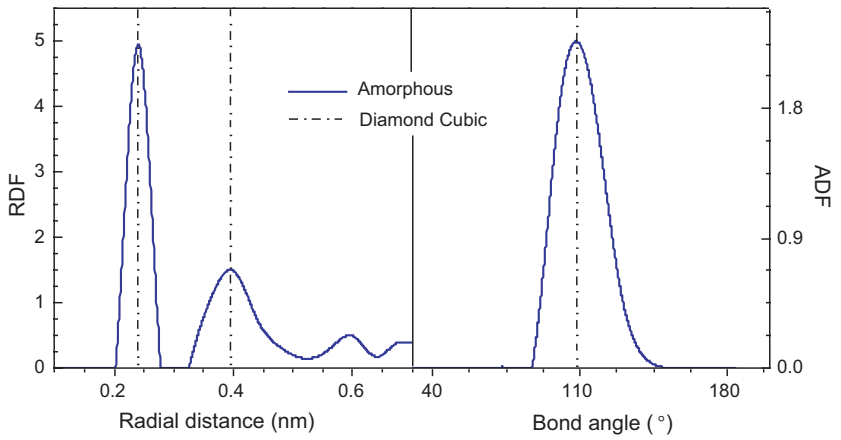

Fig. 1. Comparison of the amorphous and diamond cubic crystals of Si based on radial and angular distribution functions (RDFs and ADFs).

2. Methods

The *a*-Si structures are generated from diamond-cubic Si crystal by using an activation-relaxation technique (ART) [15]. As a computationally efficient approach, ART focuses on simulating the activated events of escaping the basins of attraction in the energy landscape, i.e., they jump over the barriers that separate different local energy minima. ART can be used to avoid the bias on structural evolution from the fast cooling rate in the melt-and-quench molecular dynamics method [16]. To speed up calculations, the *a*-Si structures are first created by using the empirical Stillinger–Weber [17] interatomic potential and then further relaxed by the Molecular Orbital PACkage (MOPAC 2009) with the AM1 method.

We adopt the protocols developed by Chevrier and Dahn [18,19] for modeling the lithium insertion and extraction. The Li atoms are randomly inserted into *a*-Si one at a time until $x = 4$. After the insertion of each Li atom, the system is fully relaxed under periodic boundary conditions; this involves the relaxation of the internal atomic coordinate, supercell size and shape. The lithium extraction process is similarly modeled. Starting from pure *a*-Si, we have repeated the insertion–extraction cycle several times, and found that the electro-mechanical responses of volume expansion and electrical potential will reach a steady state after about three cycles. To determine the electrical potential, we note that neglecting the entropy contributions [18,19], the free energy of the system can be approximated by the potential energy which is a function of atomic coordinates at zero temperature. Then the electrical potential of the Li_xSi structure versus Li/Li^+, in units of electron volts, is calculated by $V = -(dE_{Li_xSi}/dx - E_{Li})$, where E_{Li_xSi} is the potential energy of the Li_xSi structure divided by the number of Si atoms in the system and E_{Li} is the energy of a single Li atom in amorphous Li. To obtain the average responses for comparison with experimental measurements, the potential and volume are averaged over the calculation results of six statistically independent *a*-Si structures at the respective steady states. The averaging method that we used is the Savitzky–Golay smoothing filter with the main advantage of preserving features of the distribution such as relative maxima, minima and width, which are usually 'flattened' by other techniques (like moving averages, for example) [20].

3. Results and discussion

The starting amorphous structure in our calculations has 20 Si atoms. The supercell volume is 428 Å^3 corresponding to a typical density of *a*-Si, 2212 kg m^{-3} [21]. While one would like to use a larger starting system, we note that after Li insertions, the amorphous Li_xSi alloy at its charging limit involves about four times more atoms. This limits the size of the starting state because of the computational cost associated with a large number of calculations, which are necessary for averaging the voltage-composition responses and for analyzing the statistics of amorphous states. To validate the use of such a small starting system, we have generated *a*-Si with various sizes, and verified that it well represents the bulk behavior in terms of providing similar structural characteristics of the short- and medium-range order. The former can be characterized by radial and angular distribution functions (RDFs and ADFs), and the latter by ring statistics. As shown in Fig. 1, RDF has a narrow nearest-neighbor peak, while the peak of ADF centers around 109°, characteristic of tetrahedral Si bonding. These features in RDF and ADF, which are consistent with previous modeling results [21,22], indicate that the local atomic environments of *a*-Si are similar to those of atoms in the crystalline phase, as typically found in the solid-like amorphous covalent structure with a continuous random network [17].

The incorporation of Li into *a*-Si induces two kinds of structural changes that dominate at low and high Li concentrations, respectively: insertion in the interstitial hole of big rings and incorporation into the network by the destruction and reformation of small rings. We find that when the Li to Si ratio, *x*, is less than about 0.8, the added Li typically resides in the centers of the big rings after structural relaxation. This can be seen in Fig. 2(a) and (b), showing an 8-membered ring of Si (highlighted in green) before and after the insertion of one Li (in red), respectively. In this case, the big Si ring encloses a large open space and its center provides an energetically favorable interstitial site. After Li insertion, the Si–Si bonds in the ring belt do not break, but the Li atom forms new bonds with the surrounding Si atoms in the belt, causing a small adjustment of the ring geometry. Furthermore, the addition of this Li divides the big 8-membered ring into several smaller rings (three 3-membered, one 4-membered and one 5-membered rings). Consequently, the fraction of big rings in the system decreases with increasing *x*.

Fig. 2(c) and (d) shows the representative structures before and after the addition of one Li atom (in red) when $x > 0.8$. Because of the paucity of big rings, the added Li has to typically react with surrounding small rings. It pushes the nearby atoms away so as to create a larger local free volume for its incorporation into the amorphous network. In conjunction with large atomic displacements of surrounding atoms, the local ring structure is reconfigured, involving both bond breaking and formation. For example, prior to the Li addition, the length of a homopolar bond between Li atoms *e* and *b* in Fig. 2(c) is 2.69 Å. It is close to the equilibrium Li–Li bond length of 2.65 Å in the crystalline phase of $Li_{15}Si_4$ from density functional theory calculations [23]. With the addition of a Li atom (red) in

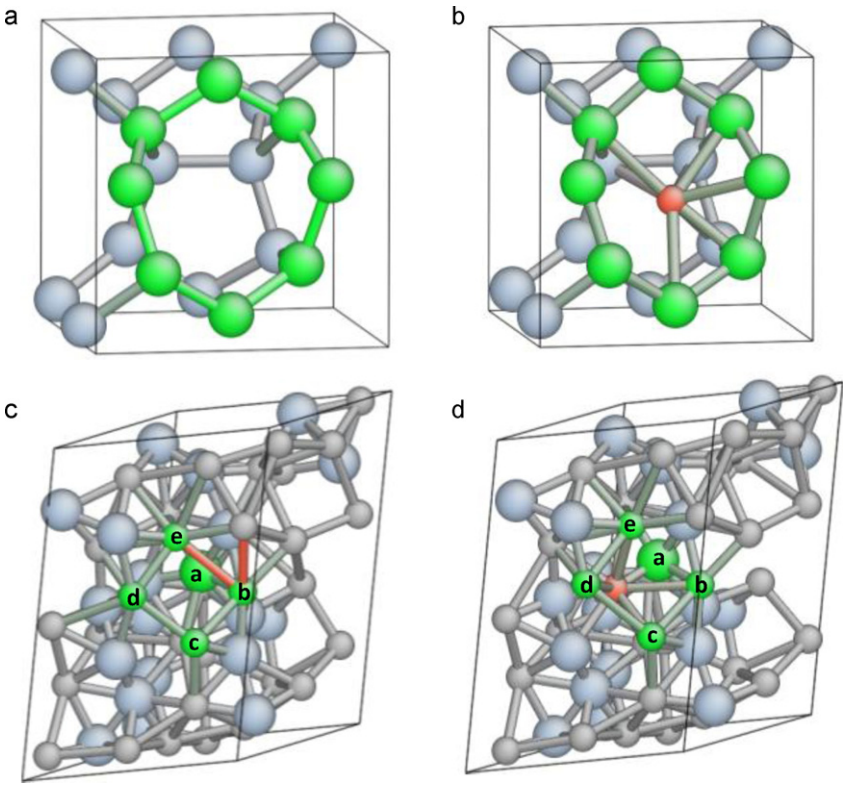

Fig. 2. Atomic structures of lithiated *a*-Si. Large and small spheres represent Si and Li, respectively. (a) and (b) Before and after the interstitial insertion of a Li atom (red) in an 8-membered ring of Si when $x = 0$. (c) and (d) Incorporation of Li into the network through breaking bonds (in red) and reformation when $x = 1.2$. (For interpretation of the references to colour in this figure legend, the reader is referred to the web version of the article.)

Fig. 2(d), both Li atoms *e* and *b* form new homopolar bonds with the inserted Li, while the bond between *b* and *e* is broken, with the separation increased to 4.05 Å. Evidently, the impact of Li insertion on the local ring structure involves the destruction of one or a few small rings with the concomitant reformation of several similar sized (3 or 4-membered) small rings.

The foregoing atomic-level structural changes associated with Li insertion can be correlated to the evolution of ring statistics, which measure the medium-range order of amorphous network structures. We use Dijkstra's shortest path algorithm [24], implemented in MATLAB, and the ring counting method developed by Franzblau [25]. As shown in Fig. 3(a), the ring fraction in the initial structure of *a*-Si ($x = 0$) exhibits a single peak at the 6-membered ring. Similar to the 8-membered ring shown in Fig. 2, this kind of big 6-membered ring provides a large open space to accommodate the interstitially inserted Li. Fig. 3(b) indicates that with increasing *x*, a peak of small 3-membered rings develops, while that of 6-membered rings diminishes. This change is understandable

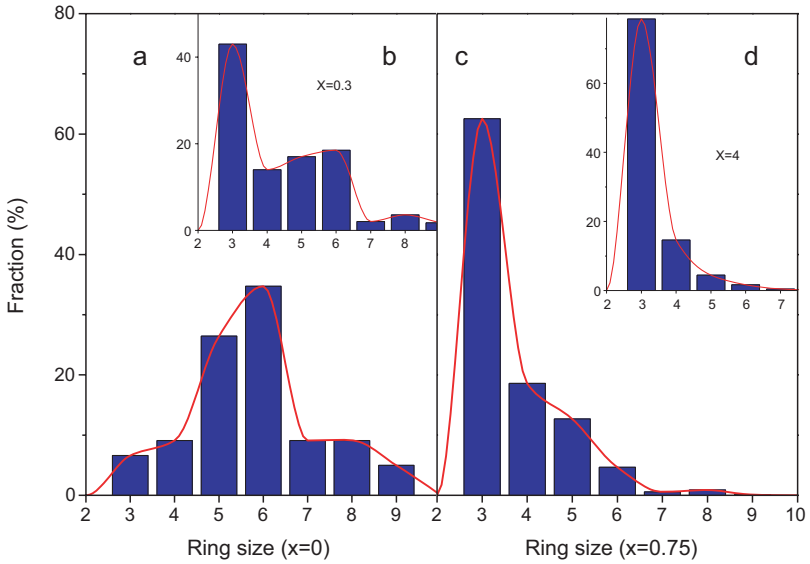

Fig. 3. Histogram of the distribution of ring size (i.e., the number of members in the ring) in lithiated *a*-Si with different ratios of Li to Si, *x*. The fitting curve (in red) is plotted to guide eyes. (For interpretation of the references to colour in this figure legend, the reader is referred to the web version of the article.)

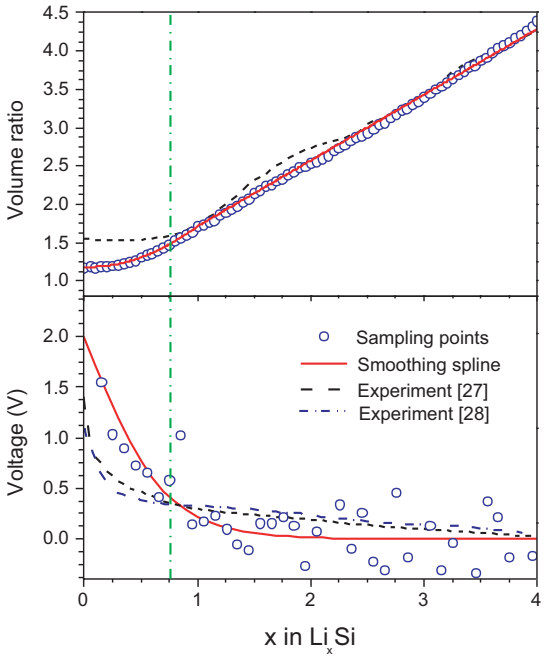

Fig. 4. Comparison of the theoretical predictions and experimental measurements [27,28] of the electro-mechanical response of lithiated *a*-Si. (a) Ratio of the current and initial volume versus Li fraction *x*; (b) voltage versus Li fraction. The red solid line represents the statistical average using the Savitzky–Golay smoothing filter [20] as discussed in Section 2. (For interpretation of the references to colour in this figure legend, the reader is referred to the web version of the article.)

by noting the earlier observation that interstitially added Li often divides the big ring into several smaller rings. Moreover, we show in Fig. 3(c) that when *x* is increased to around 0.8, the system consists dominantly of 3-membered rings with a single peak. Recall that in Fig. 2(d), a further addition of Li causes the reconstruction of local ring structures when $x > 0.8$. This can be correlated to Fig. 3(d) showing an increase of the single peak of 3-membered rings. Finally, we note that a small percentage of large rings always retain even when *x* approaches its theoretical limit. This arises because some large rings counted in the statistics correspond to the case of small rings running along the belt of the big ring [26]. These small rings occupy the open space enclosed by the ring belt. As a result, such large rings could survive because there is little room to facilitate Li insertion.

Fig. 4 shows the calculated volume and voltage versus Li composition curves, which are in accord with experimental measurements of lithiated *a*-Si [27,28]. The slope of the volume–composition curve corresponds to the volume increase per Li insertion, equivalent to the so-called partial molar volume of Li, Ω. Incidentally, Ω is a key parameter in the coarse-grained continuum model of diffusion-induced stress and cracking [9–11]. As seen from Fig. 4, Ω is small and non-linear (the numerical fitting gives $\Omega = (0.57x^2 - 0.04x + 1.18)\text{Å}^3$ per Li) when $x < 0.8$ (indicated by the green dashed line), while Ω is large and nearly a constant ($\Omega \approx 17.4\,\text{Å}^3\,\text{atom}^{-1} \approx 1.1 \times 10^{-5}\,\text{m}^3\,\text{mol}^{-1}$) as $x > 0.8$. This trend can be correlated to the foregoing analyses revealing two kinds of structural changes that dominate at low and high Li concentrations, respectively: Li interstitial insertion and incorporation into the network. In the former case, the interstitial hole can well accommodate the inserted Li, so that the induced volume expansion is relatively small. This is in contrast to the latter case where the Li incorporation occurs through network reconstruction, causing a larger volume expansion. Furthermore, the higher voltage at small *x* is related to the dominant response of bond formation between Li and Si in the ring belt, while the reduced voltage at larger *x* is attributed to the increased energy cost associated with bond breaking and stretching manifested as the increased volume expansion.

4. Concluding remarks

In summary, the present study reveals the atomic structure, volume and voltage responses of lithiated *a*-Si. The results reinforce the notion that the Li–Si alloying behavior and associated properties, including the network topology characteristics of ring statistics, are sensitive to the local Li concentration [16]. Our work provides an atomistic rational of the relatively small volume expansion when the lithium fraction is less than about 0.8. This effect arises because of the limited dilatational effect associated with the insertion of lithium atoms that mostly reside in the energetically favorable sites of interstitial holes in the open network structure of Si. Since such small volume expansion has an intrinsic atomistic structural basis, it may have implications for reducing the stress buildup and thereby improving the reversibility of charging and discharging processes by controlling the extent of lithiation.

While the work focuses on the static aspects of lithiation, it also has implications on the dynamic processes of Li–Si mixing and electrochemically driven solid state amorphization. Consider, as an example, Li diffusion in *a*-Si that underlies the aforementioned processes. It is generally recognized that diffusion in amorphous materials is controlled by a distribution of energy minima and activation barriers associated with a disordered network. This has been revealed, for example, in the study of oxidation of Si [29,30] and hydrolysis of silica [31]. The present analyses of Li insertion in *a*-Si and, in particular, the calculated ring statistics suggest a simplified view of the energy landscape governing the Li diffusion and mixing in *a*-Si. Namely, the interstitial holes represent the deep sites (i.e., valleys) in the energy landscape, and the network incorporation sites correspond to the shallow sites. The deep and shallow sites can be, respectively, related to the 6-membered and 3-membered rings that peak in the ring distribution function at different *x* values (Fig. 3). While the deep sites may play an important role in the volume and voltage changes during lithiation, the rate of Li diffusion is likely to be governed by the shallow sites with low activation barriers between neighboring shallow ones and by their percolation in the disordered network. A mechanistic study of the dynamic lithiation process would be highly desirable via a multiscale model that incorporates the above insights, e.g., by coupling the atomistic barriers, network topology and kinetic Monte-Carlo sampling, as implemented in the Si oxidation simulation [30]. This is important for understanding the electrochemical alloying, and could have implications on improving the energy density and cycle reversibility of Li-ion batteries.

Acknowledgments

We acknowledge the support from the National Science Foundation grant CMMI-0758554. Discussions with Yue Qi, Min Zhou and Yifan Gao have been helpful.

References

[1] J.M. Tarascon, M. Armand, Nature 414 (2001) 359.
[2] J.M. Tarascon, Philosophical Transactions of the Royal Society A 368 (2010) 3227.
[3] L.Y. Beaulieu, K.W. Eberman, R.L. Turner, L.J. Krause, J.R. Dahn, Electrochemical and Solid State Letters 4 (2001) A137.
[4] P. Limthongkul, Y.I. Jang, N.J. Dudney, Y.M. Chiang, Acta Materialia 51 (2003) 1103.
[5] J. Graetz, C.C. Ahn, R. Yazami, B. Fultz, Journal of the Electrochemical Society 151 (2004) A698.
[6] C.K. Chan, H.L. Peng, G. Liu, K. McIlwrath, X.F. Zhang, R.A. Huggins, Y. Cui, Nature Nanotechnology 3 (2008) 31.

[7] T. Song, J.L. Xia, J.H. Lee, D.H. Lee, M.S. Kwon, J.M. Choi, J. Wu, S.K. Doo, H. Chang, W. Il Park, D.S. Zang, H. Kim, Y.G. Huang, K.C. Hwang, J.A. Rogers, U. Paik, Nano Letters 10 (2010) 1710.
[8] R. Chandrasekaran, A. Magasinski, G. Yushin, T.F. Fuller, Journal of the Electrochemical Society 157 (2010) A1139.
[9] R.A. Huggins, W.D. Nix, Ionics 6 (2000) 57.
[10] T.K. Bhandakkar, H.J. Gao, International Journal of Solids and Structures 47 (2010) 1424.
[11] Y.H. Hu, X.H. Zhao, Z.G. Suo, Journal of Materials Research 25 (2010) 1007.
[12] C.J. Wen, R.A. Huggins, Journal of Solid State Chemistry 37 (1981) 271.
[13] T. Zhu, J. Li, Progress in Materials Science 55 (2010) 710.
[14] M.J.S. Dewar, E.G. Zoebisch, E.F. Healy, J.J.P. Stewart, Journal of the American Chemical Society 107 (1985) 3902.
[15] G.T. Barkema, N. Mousseau, Physical Review Letters 77 (1996) 4358.
[16] V.B. Shenoy, P. Johari, Y. Qi, Journal of Power Sources 195 (2010) 6825.
[17] F.H. Stillinger, T.A. Weber, Physical Review B 31 (1985) 5262.
[18] V.L. Chevrier, J.R. Dahn, Journal of the Electrochemical Society 156 (2009) A454.
[19] V.L. Chevrier, J.R. Dahn, Journal of the Electrochemical Society 157 (2010) A392.
[20] A. Savitzky, M.J.E. Golay, Analytical Chemistry 36 (1964) 1627.
[21] M.J. Demkowicz, A.S. Argon, Physical Review Letters 93 (2004) 025505.
[22] N. Mousseau, G.T. Barkema, Physical Review B 61 (2000) 1898.
[23] Y. Kubota, M.C.S. Escano, H. Nakanishi, H. Kasai, Journal of Applied Physics 102 (2007) 053704.
[24] E.W. Dijkstra, Numerische Mathematik 1 (1959) 269.
[25] D.S. Franzblau, Physical Review B 44 (1991) 4925.
[26] S. Caravati, M. Bernasconi, M. Parrinello, Physical Review B 81 (2010) 014201.
[27] L.Y. Beaulieu, T.D. Hatchard, A. Bonakdarpour, M.D. Fleischauer, J.R. Dahn, Journal of the Electrochemical Society 150 (2003) A1457.
[28] L. Baggetto, J.F.M. Oudenhoven, T. van Dongen, J.H. Klootwijk, M. Mulder, R.A.H. Niessen, M. de Croon, P.H.L. Notten, Journal of Power Sources 189 (2009) 402.
[29] N.F. Mott, Philosophical Magazine B 55 (1987) 117.
[30] A. Bongiorno, A. Pasquarello, Physical Review B 70 (2004) 195312.
[31] T. Zhu, J. Li, X. Lin, S. Yip, Journal of the Mechanics and Physics of Solids 53 (2005) 1597.